Astron. Astrophys. 305, 887–901 (1996)

ASTRONOMY AND ASTROPHYSICS

Long-term spectroscopic monitoring of BA-type supergiants

I. H_α line-profile variability*

A. Kaufer[1], O. Stahl[1], B. Wolf[1], Th. Gäng[1], C.A. Gummersbach[1], J. Kovács[2], H. Mandel[1], and Th. Szeifert[1]

[1] Landessternwarte Heidelberg-Königstuhl, D-69117 Heidelberg, Germany
[2] Gothard Astrophysical Observatory, H-9707 Szombathely, Hungary

Received 28 January 1995 / Accepted 19 May 1995

Abstract. We have obtained time series of spectra in the wavelength range 4 000 – 6 800 Å over several months with high S/N and high resolution in wavelength ($\lambda/\Delta\lambda \approx 20\,000$) and time ($\Delta t \approx 1$ d) of the late-type B and early-type A supergiants HD 91619 (B7 Ia), βOri (B8 Ia), HD 96919 (B9 Ia), HD 92207 (A0 Ia), HD 100262 (A2 Ia) and αCyg (A2 Ia). H_α is found to show broad emission extended to about $\pm 1\,200$ km s^{-1} for all objects except αCyg. Due to the lack of strong line-emission in H_α the electron-scattered photons are expected to originate in deep atmospheric layers. In all of the objects the H_α-line profiles are found to be highly variable on different time scales reaching from days to months. Patterns of variation in H_α are found to be quite symmetric about the systemic velocity and are mainly due to variable blue and red-shifted emission superimposed on almost constant photospheric and/or wind profiles. These V/R variations are interpreted in terms of axial symmetry of the envelopes of these objects. Time-series analyses of the variations reveal H_α time scales up to a factor of 6 longer than expected radial fundamental pulsation periods but consistent with rotational periods. Therefore, rotational modulation as a possible source of variability is concluded. Corotating weak magnetic surface structures are suggested as the source for a rotationally modulated lower wind region. Suddenly appearing deep and highly blue-shifted absorptions in H_α are ascribed to instabilities of the ionization structure of the wind. Outwards propagating discrete absorption components have been observed only once in HD 92207.

Key words: stars: early-type; supergiants; emission-line; rotation; oscillations

1. Introduction

Compared to the wealth of data accumulated for luminous OB stars studies of photospheric and wind properties of late B-type and early A-type supergiants (which we will call BA-type supergiants in the following) are still scarce. One of the most interesting properties of these objects is their variability, which was found in a spectroscopic study of radial velocities of the prototype of the class, αCyg, by Paddock (1935) already 60 years ago. This intrinsic variability of BA-type supergiants – as for the O stars – is expected to be the key to a detailed understanding of the underlying physical mechanisms in their atmospheres. Therefore the aim of this study is to provide the observational material for such investigations.

The relevant time scales associated with the variability are of the order of days to months, which so far has prevented continuous observations with high-resolution spectroscopy hitherto only available at large telescopes with high pressure factors. However, with the advent of fiber-linked echelle spectrographs in combination with efficient CCDs bright stars are in the reach of sub-meter class telescopes.

1.1. Variability and time scales

BA-type supergiants have been known as photometric and optical spectrum variables for a long time:

In the fundamental works of Abt (1957) and Rosendhal & Wegner (1970a, 1970b) semiperiodic radial velocity, line intensity, and width variations with typical time scales from 5 to 50 days were discussed in the context of line-broadening mechanisms such as rotation and photospheric velocity fields like expansion, macroturbulence and depth-dependent microturbulence; the latter in detail for αCyg by Groth (1972).

Lucy (1976) concluded from his period analysis of the already mentioned radial velocity curves obtained for αCyg by Paddock (1935) the simultaneous excitation of multiple pulsational modes including radial modes and low-order non-radial g modes. Gautschy (1992) in his non-adiabatic stability analy-

Send offprint requests to:
A. Kaufer *e-mail*: akaufer@hp2.lsw.uni-heidelberg.de

* Based on observations collected at the European Southern Observatory at La Silla, Chile, and observations by the International Ultraviolet Explorer collected at the Villafranca Satellite-Tracking Station of the European Space Agency

ses found excitation of modes in the frequency range of Lucy's work but had to adopt a very low mass for αCyg ($\approx 6.5\ M_\odot$).

From photometric long-term monitoring projects Maeder & Rufener (1972), Sterken (1976), and Burki (1978) were able to derive typical time scales ('semiperiods') for variations of supergiants similar to those derived from radial velocities. Their constructed (semi)period-luminosity functions show the same slope as the P-L function of the Cepheids interpreted as an indication for the pulsational nature of the observed light variations. This was also supported by models of Lovy et al. (1984). The systematic discrepancy between the models and the observations in the sense that observed semiperiods are longer than the computed periods of radial fundamental modes was ascribed to the existence of non-radial g modes.

The H_α-emission survey by Rosendhal (1973b) of early-type high-luminosity stars revealed H_α emission with P Cyg profiles for all of the most luminous B8–A3 stars indicating stellar wind and mass-loss. A large variety of H_α profiles was observed: pure absorption, classical and inverse P Cyg profiles but also double-peaked emission profiles. If visible, the emission components were red-shifted with respect to the metallic lines between 50 and 100 km s^{-1}, sometimes with a blue emission counterpart being symmetric in velocity.

In a preceding work Rosendhal (1973a) had discovered variable H_α profiles from snapshot observations with intervals of several years. Thus only the variability itself was noted but neither typical time scales for H_α variability nor connections to photospheric variability (Rosendhal 1972) could be examined.

Wolf & Sterken (1976) stated from H_α sequences of HD 91619 (B7 Ia) and HD 96919 (B8 Ia) Be-star characteristics with V/R variability. Baade (1988b) found cyclic H_α variations for early B-type supergiants showing signs for non-spherical symmetry. The observed variations were explained by matter lifted in each cycle above the star and then slowly dispersed and accelerated in the wind, partially also returned to the star. From simultaneous observations of H_α and the nearby C II lines cyclic behavior for the latter photospheric lines was stated, too, but no correlation to the H_α variations. 'The profile variations [of C II] are not dissimilar to the effects of low-order non-radial pulsations'.

In the UV range Lamers & Stalio (1978) and Talavera & Gomez de Castro (1987) observed blue-shifted metallic lines (Fe II) and stable wind profiles in the resonance lines Fe II and Mg II — clear signs for a continuous outflow with constant terminal velocities. Weak variability was observed in form of discrete absorption components (DACs) in the resonance lines. Underhill & Fahey (1984) have proposed that these DACs may be caused by the release of parcels of gas from localized regions above the stellar photosphere. Further, it is inferred that the release mechanism of this localized ejection is associated with bipolar magnetic regions on the surface of the star.

1.2. Problems and perspectives

From the above arguments the main outstanding problems for a better understanding of the outer atmospheres of BA-type supergiants can be summarized as follows:

1. No detailed study of photospheric and wind variability with sufficient time coverage and resolution is available.
2. The evolution of H_α line profiles, time scales, and sources of H_α variability are unknown.
3. The rôle of radial and non-radial pulsations for photospheric variability is not clarified.
4. No connection of photospheric variability to wind variability and variable mass-loss is established.

If further insight could be gained, BA-type supergiants would be important test objects for the theory of time-dependent radiation-driven winds of BA supergiant stars and the theory of evolution of massive stars with special attention to the model predictions for pulsational instability (e.g. Kiriakidis et al. 1993).

2. Spectroscopic monitoring

The limited knowledge of the behaviour of BA-type supergiants compared to early-type supergiants is mainly caused by the insufficient quality and density of observations over long time spans. Therefore we initiated a spectroscopic long-term monitoring project for bright late B-type and early A-type supergiants. We tried to fulfil the following requirements to optimize the gain of information to be extracted from the spectra:

large spectral range to allow an examination of the depth structure of the transition zone photosphere – wind by spectral lines formed in various regions of the atmosphere, including H_α as the most sensitive wind indicator in the optical spectral range,

high S/N and *high spectral resolution* to provide sufficient accuracy for radial velocity measurements (≈ 1 km s^{-1}) and definition of line profiles (≈ 1 %),

monitoring over *long time spans* (months) with *high time resolution* (days) to account for the different time scales of variations expected in the photosphere and the envelope, respectively from object to object. *Repetitions* of such monitoring campaigns over several years give information on the stability of observed phenomena and on variations on still longer time scales.

3. Observations

3.1. The sample

The sample of BA-type supergiants selected for the monitoring program is shown in Table 1 together with coordinates, visual magnitude V, and spectral type *sp*. The selection criteria for this sample were primarily the spectral type, the luminosity class, and the brightness of the object. All objects were known to be photometric and/or spectroscopic variables before (cf. Wolf &

Table 1. List of monitored BA-type supergiants

Object	α (1950)	δ (1950)	V	sp
HD 91619	10 33 25.3	–58 11 25	6.14	B7 Iae
HD 34085 (βOri)	05 14 32.2	–08 12 06	0.12	B8 Iae
HD 96919	11 08 33.8	–61 56 49	5.13	B9 Iae
HD 92207	10 37 26.8	–58 44 00	5.45	A0 Iae
HD 100262	11 31 48.6	–59 30 56	5.15	A2 Iae
HD 197345 (αCyg)	20 39 43.5	+45 06 03	1.25	A2 Iae

Table 2. The αCyg campaigns in Heidelberg

Object	spectra/nights 1990	1991	t_{exp} [min]	S/N
HD 197345	49/173	74/155	10	350

Sterken 1976 and Sterken 1976 for the southern objects, Sanford 1947 for βOri, Paddock 1935 and Fath 1935 for αCyg). Futher, all objects are believed to be single stars.

3.2. The instrument

All optical spectra in this work were taken with FLASH, the **F**iber **L**inked **A**stro Echelle **S**pectrograph of **H**eidelberg (Mandel 1988) equipped with an EEV - CCD (1152×770, 22 μ pixel) and an optical fiber of 100 μm core diameter, which provides a spectral resolution of $R = \lambda/\Delta\lambda \approx 20\,000$. In one exposure a wavelength range from 4 000 to 6 800 Å is covered on 58 echelle orders.

Due to the mechanical separation of the spectrograph from the telescope, excellent stability is guaranteed during the night. Fiber-fed calibration exposures of an internal flatfield lamp and a Thorium-Argon hollow-cathode lamp for wavelength calibration are taken in intervals of two hours.

3.3. The campaigns

For the first campaigns on the prototypical A supergiant αCyg in 1990 and 1991 we used the 70-cm telescopes of the Landessternwarte in Heidelberg. Despite the moderate weather conditions in Central Europe it was possible to gather numerous spectra with partially good time coverage in those two seasons.

For the monitoring of the southern objects we had so far one campaign of 30 nights in July 1992 and two further campaigns in 1993 (120 nights, February to May) and 1994 (150 nights, February to June with an interruption of two weeks in April) at the European Southern Observatory at La Silla, Chile. The spectrograph was primarily attached to the ESO 50-cm telescope (cf. Wolf et al. 1993) but also to the Bochum 60-cm telescope for three weeks in 1994. Excellent time coverage, with nearly one spectrum per night, was achieved due to the outstanding weather conditions at this site. A résumé of the observations with the number of spectra obtained for each object and campaign is given along with the typical exposure times in minutes in Tables 2 and 3. As a measure for the achieved quality the typical S/N in V is listed, too.

Table 3. The La Silla campaigns

Object	spectra/nights 1992	1993	1994	t_{exp} [min]	S/N
HD 91619	–	–	52/60	120	100
HD 34085	20/27	86/104	88/90	5	350
HD 96919	–	83/116	102/130	60	150
HD 92207	–	86/115	107/129	60	120
HD 100262	–	–	98/130	60	150

3.4. The data reduction

The FLASH spectra were reduced semi-automatically using a modified version of the MIDAS[1] *echelle* context (cf. Stahl et al. 1993). For the flatfield correction and wavelength calibration the corresponding spectra of each night are checked for shifts on the detector. The largest shifts found in direction of main dispersion and cross dispersion are of the order of half a pixel. This exceeds the reachable internal accuracy of one third of a pixel, which is about 1 km s^{-1} if translated into radial velocities in the final reduced spectra. Therefore if larger shifts occur, the night is divided into two or more sections, for which the reductions are performed independently. Flatfields are averaged mainly to achieve a sufficiently high S/N especially in the blue region, which is limited by the flux from the flatfield lamp. For the wavelength calibration the averaged frame is used, too. The echelle orders of the object and calibration frames are extracted into two-dimensional pixel-order frames. Dispersion coefficients are found in the Thorium-Argon pixel-order frame according to the method described by Hensberge & Verschueren (1990). Flatfielding is also done in the pixel-order regime utilizing the fact that all frames were obtained through the same fiber, i.e. the same light path within the spectrograph. Hence, as one of the most important advantages of fiber-fed spectrographs, no ripple correction has to be applied to the spectra anymore. Finally, the resulting wavelength-calibrated and flatfielded spectra are merged, rebinned to heliocentric velocities at half time of the exposure, and normalized by a spline fit to the continuum through predefined continuum windows.

The long-term accuracy achieved for the wavelength calibration is of the order of 1 km s^{-1} as derived from the spread of measured radial velocities of telluric lines in the spectra. The continuum determination for hot stars mainly suffers from the remaining ripples in the spectra, which have maximum amplitudes of about 1 % relative to continuum.

4. Stellar parameters

Table 4 gives a compilation of the basic parameters for the stars in the sample. The sequence in spectral type, i.e. in temperature, was verified by measuring the ratio of the mean equivalent widths of Mg IIλ4481 and He Iλ4471. Due to the large spread of the measurements in the literature it was decided to derive the absolute visual magnitude M_V in an uniform way from

[1] **M**unich **I**mage **D**ata **A**nalysis **S**ystem, European Southern Observatory

the obtained spectra using the calibration of Azzopardi (1981), which connects M_V with the measured equivalent width W_λ of H_γ and the spectral type *sp*. $W_\lambda(H_\gamma)$ measurements were performed for all spectra available by integration in fixed limits of ± 9 Å. Averages are given for all objects in the table. The spread in measured $W_\lambda(H_\gamma)$ is of the order of 5 %, which is the expected internal accuracy. For HD 96919 and HD 92207 values of 20 % are reached, which has to be attributed to intrinsic stellar variability. The bolometric correction $B.C.$ and the effective temperature $T_{\rm eff}$ according to the spectral type are taken from Schmidt-Kaler (1982); the mass $M/M_\odot$ is interpolated from evolutionary tracks of Schaller et al. (1992) assuming that the star is evolving to cooler temperatures.

For a later discussion of the observations, estimates of the relevant velocities and time scales are useful. Therefore the computed break-up velocities $v_{\rm break}$ and corresponding rotational periods $P_{\rm rot,break}$ are given. Escape velocities are derived with $\Gamma = \frac{\sigma_e L}{4\pi cGM}$ and an adopted value of $\sigma_e = 0.33$, which assumes solar abundances and continuous opacity due solely to electron scattering.

Terminal velocities $v_{\rm inf}$ were measured from high-resolution IUE spectra as shown in Fig 1. For the spectral types later than B9, $v_{\rm inf}$ is well defined by the blue edge of the resonance lines Mg IIλ2795 and Mg IIλ2803 determined as the intersection of the extrapolated blue edge of the lines and an interpolated continuum. In the cases of HD 96919 and βOri the measured values for $v_{\rm inf}$ are lower limits only because no sharp blue edge is observed but a quite symmetric blue-shifted absorption. In fact, e.g. Gilheany (1991) reports the detection of discrete absorption components extending to -400 km s^{-1} in βOri. The terminal velocities $v_{\rm inf}$ and the velocities at half minimum (in brackets) given in the table are corrected for the systemic velocities (see below) and for the uncertainties in the wavelength calibration of the IUE spectra by measuring the velocity shift between the interstellar Mg Iλ2852 UV line and the Na I doublet in the well-calibrated optical spectra.

Projected rotational velocities $v \sin i$ can be estimated from the width of the line-profile variations of photospheric lines. According to Reid et al. (1993) $v \sin i$ was defined as the maximum half-width of features in the 'temporal variance spectra' (TVS) (cf. Sect. 7.2). We used the two strong isolated absorption lines Si IIλ6347 and Fe IIλ5169, which show nicely-defined (double-peaked) features with steep flanks in the TVS. The mean measured values are given in column $v \sin i$ of Table 4. The achieved accuracy for $v \sin i$ is primarily limited by the contribution of the projected radial components of the pulsation-like motions to the width of the features in the TVS. As discussed below, this contribution is found to be of the order of some 5 km s^{-1}, which is still small compared to the values for $v \sin i$. From $v \sin i$ and $v_{\rm break}$ we get an upper and lower limit for the true rotational periods of the star, that is $P_{\rm rot}/\sin i$ and $P_{\rm rot,break}$.

A further important intrinsic time scale of the star is the radial fundamental pulsation period. $P_{\rm rad,fund}$ was computed according to Lovy et al. (1984) for a pulsation constant $\log Q = -1.4$, which they found to be valid in the regime of

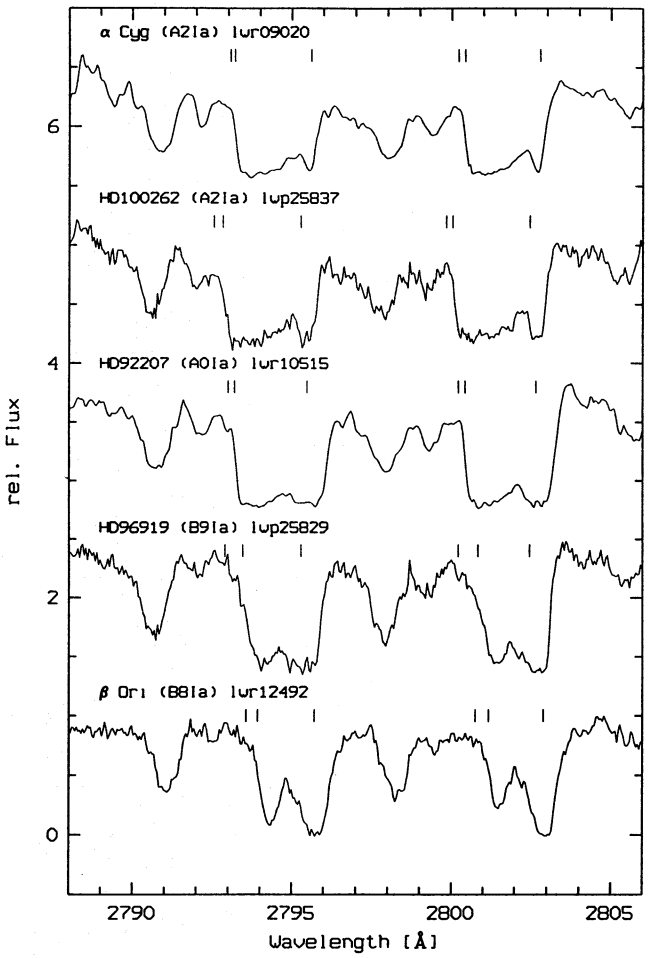

Fig. 1. Representative spectra of the objects βOri, HD 92207 and αCyg from the IUE archives and of HD 96919 and HD 100262 observed by us are used for the determination of terminal velocities $v_{\rm inf}$. The measured positions of $v_{\rm inf}$ and the velocity at half minimum along with the systemic velocity are indicated by vertical bars on top of the resonance lines Mg IIλ2795 and Mg IIλ2803

BA supergiants. It should be noted that the derived pulsation periods for our sample lie well below the lower limit of the rotational periods, and therefore the possibility of a discrimination between rotation and pulsation as sources of stellar variability arises in contrast to early-type OB stars.

A determination of the systemic velocities $v_{\rm sys}$ is indispensible for the interpretation of all absolute velocities to be discussed. Therefore we used a set of selected photospheric lines from the line list of Kurucz & Peytremann (1975) and measured their radial velocities in all available spectra for each object. Averaged radial velocities are given in column $v_{\rm sys}$. The found spread of typically 5 km s^{-1} in radial velocities must be attributed to intrinsic stellar radial velocity (= line-profile) variations because the reached instrumental accuracy in our spectra is about 1 km s^{-1} and no strong depth dependence of the radial velocities in this set of lines was found. A detailed discussion of the photospheric variability will be given in a forthcoming paper.

Table 4. Stellar parameters of the sample derived from spectral type and equivalent width of H_γ with the calibration of Azzopardi (1981). Masses are interpolated from evolutionary tracks of Schaller et al. (1992). For a discussion of the derived velocities and periods cf. Sect. 4

Object	*sp*	W_λ(Mg4481)/ W_λ(He4471)	$W_\lambda(H_\gamma)$ [Å]	M_V	*B.C.*	M_{bol}	$\log L/L_\odot$	T_{eff} [K]	$R/R_\odot$	$M/M_\odot$	$\log g$
HD 91619	B7	0.8	1.43	–7.99	–0.78	–8.77	5.42	12 200	114	27	1.75
HD 34085	B8	1.2	1.64	–7.77	–0.66	–8.43	5.28	11 200	116	23	1.67
HD 96919	B9	2.5	1.56	–7.97	–0.52	–8.49	5.30	10 300	141	23	1.50
HD 92207	A0	4.6	1.34	–8.29	–0.41	–8.70	5.39	9 730	174	23	1.32
HD 100262	A2	5.9	2.60	–7.50	–0.28	–7.78	5.02	9 080	131	18	1.46
HD 197345	A2	6.3	2.80	–7.30	–0.28	–7.58	4.94	9 080	119	18	1.54

Object	v_{break} [km/s]	$P_{rot,break}$ [d]	$\sqrt{1-\Gamma}$	v_{esc} [km/s]	v_{inf} [km/s]	$v \sin i$ [km/s]	$P_{rot}/\sin i$ [d]	$P_{rad,fund}$ [d]	v_{sys} [km/s]
HD 91619	212	27	0.87	261	–	60	96	9	–6
HD 34085	195	30	0.89	244	< –229(–187)	55	107	10	+18
HD 96919	176	40	0.88	220	< –249(–186)	60	119	14	–24
HD 92207	159	55	0.85	192	–263(–242)	55	160	19	–17
HD 100262	162	41	0.92	212	–287(–262)	50	132	14	–17
HD 197345	170	36	0.94	225	–262(–254)	50	121	12	–1

5. Detections in the averaged spectra

With the large number of spectra obtained it is possible to detect weak spectral features in the extremely high signal-to-noise averaged spectra (cf. Stahl et al. 1993).

5.1. Emission lines

We have found in our sample three weak and so far unidentified emission lines. Apart from H_α no emission has been seen in the spectra of BA-type supergiants. An examination of the time series of the individual spectra reveals that these emission lines do not show a run with time due to the heliocentric correction of the spectra like the telluric lines, which excludes a terrestrial origin for these emission lines. Table 5 gives the measured wavelengths and the wavelengths λ_{cor}, which were corrected with the systemic velocities of the object along with the measured equivalent widths and FWHM of the lines. The wavelengths were finally determined to 5593.27 ± 0.09 Å, 6172.66 ± 0.14 Å and 6318.21 ± 0.10 Å. An identification of these lines and the emission mechanism is desirable to judge their diagnostic value.

5.2. Extended emission wings around Hα

Fig. 2 displays the averaged spectra of 1993 and 1994 around H_α. Broad emission wings are clearly discernible for all BA-type supergiants except for αCyg. This is especially remarkable because of the very weak central emission in HD 91619, βOri, and HD 96919, which usually is thought to be the source of line photons distributed into the wings by electron scattering. The emission rises up to 10 % above the continuum and is for all objects extended to about $\pm 1\,200$ km s^{-1} in velocity.

Extensive emission wings have been presented by Ebbets (1982) for some early-type supergiants, which he primarily attributed to the high expansion velocities in their stellar winds. This cannot hold for these BA supergiants because the terminal velocities of about $200 - 400$ km s^{-1} are much below the velocities reached in the emission wings.

The NLTE effect described by Hubeny & Leitherer (1989) can only account for wings extending to widths according to the Stark broadening, which are of the order of $300-500$ km s^{-1} for H_α. However, their NLTE emission mechanism working in deep atmospheric layers may account for the neccessary deep-seated H_α emission, which then could be dispersed by the traditional electron-scattering mechanism in higher layers into emission wings of the observed widths.

6. Dynamical spectra

Due to the large number of spectra obtained it is necessary to find an appropriate representation for the time series of spectra. As can be seen in Figs. 3–8 we use so-called dynamical spectra for this purpose. They were implemented in the MIDAS environment as follows: in a first step a set of time-ordered spectra is rebinned to velocities within a chosen interval with the zero-point set to a specific wavelength, e. g. the laboratory wavelength of the spectral line of interest. To take into account for the uneven sampling in time, the spectra are interpolated with splines and resampled to a chosen time step at each velocity. If a gap between two observations exceeds three time steps the dynamical spectrum is left black in this time span. Finally the intensities are coded in grey scales (from black = absorption to white = emission), which leads to a two-dimensional velocity–time frame. At the right ordinate of this frame the dates of exposure of the contributing spectra are marked.

Above the dynamical spectra, all spectra are plotted within a wavelength range corresponding to the velocity range and an appropriate intensity interval to display clearly the fluctuations at specific velocities. The cut values used for the grey-scale representation are indicated by broken lines, the grey scale itself is shown at the right-hand side and may be used as a look-up table for the intensities.

Table 5. Detected weak emission lines. The measured wavelengths λ were corrected with the estimated systemic velocities of the objects and are given in column λ_{cor}. b = blended by nearby absorption line, c = blended by crossing telluric line, d = disturbed by defect, – = feature not found. The mean values of all λ_{cor} are given with their standard deviations

Object	year	λ5593				λ6172					λ6318				
		λ [Å]	λ_{cor} [Å]	W_λ [mÅ]	FWHM [Å]	λ [Å]	λ_{cor} [Å]	W_λ [mÅ]	FWHM [Å]		λ [Å]	λ_{cor} [Å]	W_λ [mÅ]	FWHM [Å]	
HD 91619	1994	5593.06	5593.17	12	1.2	–	–	–	–		6318.04	6318.17	11	0.7	
	1993	5593.64	5593.30	10.7	1.0	6172.99	6172.62	5.3	1.0	b	6318.44	6318.06			c
HD 34085	1994	5593.57	5593.23	10.8	1.1	6172.88	6172.51			d	6318.54	6318.16			c
	1993	5592.83	5593.27	10	1.0	6172.06	6172.55	10	1.0		6317.76	6318.26	13	0.8	
HD 96919	1994	5592.85	5593.30	11	1.1	6172.27	6172.76	11	1.0		6317.72	6318.23	13	0.7	
	1993	5592.98	5593.30	9	1.1	6172.23	6172.58	9	0.8						c
HD 92207	1994	5593.00	5593.32	10	1.1	6172.46	6172.81	13	1.0		6318.00	6318.36	5	0.5	c
HD 100262	1994	–	–	–	–	6172.51	6172.93	5	0.9						b
	1990	–	–	–	–	6172.58	6172.60	5	1.0						b
HD 197345	1991	–	–	–	–	6172.60	6172.62	5	1.1						b
Mean		5593.27 ± 0.09 Å				6172.66 ± 0.14 Å					6318.21 ± 0.10 Å				

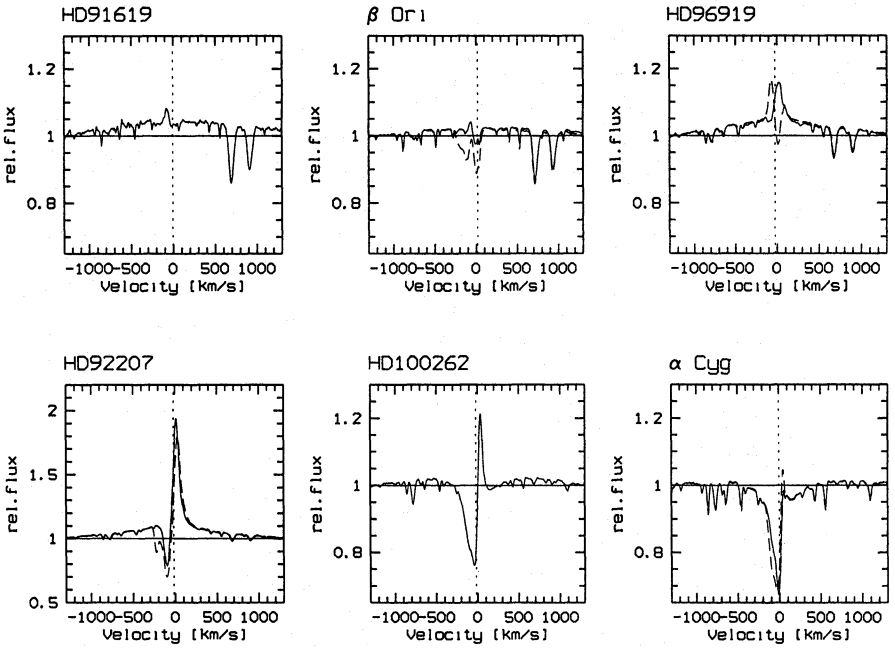

Fig. 2. Averaged spectra around H_α showing broad emission wings extended to ±1 200 km s^{-1}. Solid lines = 1993 (1990 for αCyg), dashed lines = 1994 (1991 for αCyg). Consider the different scaling in the ordinate for HD 92207

7. H_α line-profile variations

The H_α line is the most sensitive tracer of the stellar wind in the optical spectral range of BA supergiants. H_α is the only spectral line showing emission components in an otherwise purely absorption-line spectrum – with the exception of the weak emission lines discussed in Sect. 5. From the well-established fact that these stars suffer from moderate mass-loss it would be expected to find P Cyg-type profiles in H_α.

In Figs. 3 – 8 the dynamical spectra of H_α are presented for all monitored objects. If data from two years are available the dynamical spectra are stacked keeping the scales for time and velocity axes fixed.

The spectral region around H_α is contaminated by telluric water-vapour lines. Fortunately they can easily be identified in the dynamical spectra as sharp absorptions varying in depth and position (e.g. clearly visible in the lower dynamical spectrum in Fig. 4 around −240 and −280 km s^{-1}). Note the smooth curvature of these telluric lines due to the reduction of the spectra to heliocentric velocities, which also demonstrates the accuracy of the radial velocities.

7.1. General appearance

In all objects the H_α-line profiles are found to be highly variable on different time scales reaching from days to months. If differences in the appearance of profiles from year to year or observations of events that have so far been observed only once are also considered, even longer time scales are indicated.

The patterns of variation are characterized by blue and red-shifted emission and blue and red-shifted absorption for the objects showing no clear P Cyg profile in H_α, i.e. *HD 91619*

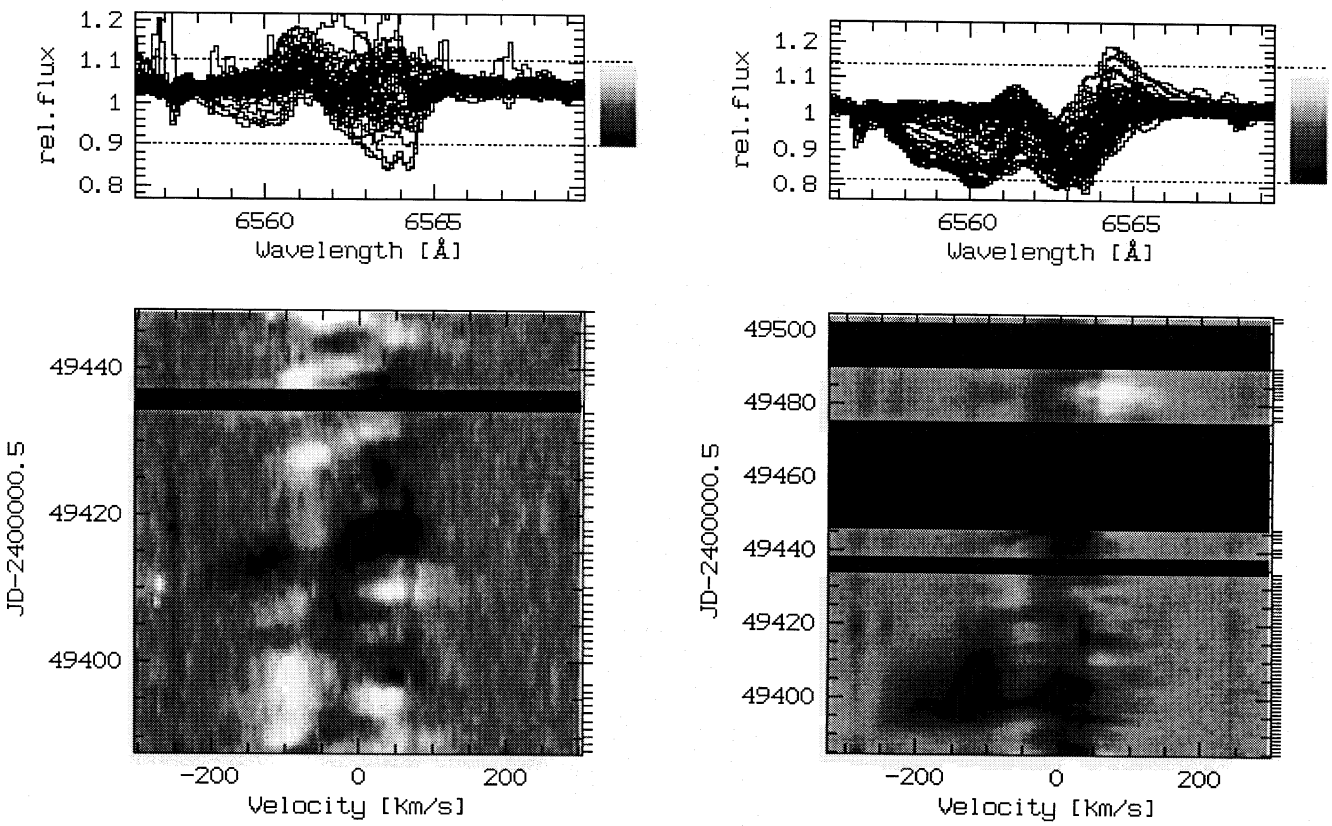

Fig. 3. Dynamical spectrum of H_α of HD 91619 in 1994

(Fig. 3), *βOri* (Fig. 4), and *HD 96919* (Fig. 5). Especially variable emission close to the borders of the region of variability – typically extended to ± 100 km s^{-1} – is strongly reminiscent of the classical V/R variations in Be stars but obviously not physically connected because the time scales observed for the V/R variations of the BA-type supergiants (days) are several orders of magnitude shorter than in Be stars where V/R variations occur on time scales of years. Variations of this kind are hard to understand in terms of intrinsic or photospherically triggered variations in a spherically symmetric wind. Especially the appearance of red-shifted absorption and blue-shifted emission and the lack of features propagating outwards on the blue side of the profile would be hard to understand in such a scenario. On the other hand, double-peaked emissions with V/R variations are in a quite natural way interpreted in terms of deviations from spherical symmetry, i.e. stellar disks or axial symmetry in general.

In the case of *αCyg* (Fig. 8) a clear P Cyg profile is present. A closer look at the velocity axis shows that the minimum of the profile falls close to the systemic velocity of -1 km s^{-1} whereas the red emission is located at about +20 km s^{-1}. Therefore, this H_α feature has to be interpreted as consisting of a variable red emission component superimposed upon a photospheric absorption profile that has extended wings and is centered at systemic velocity. Almost symmetric to the red emission with respect to the systemic velocity a variable component at -60 km s^{-1} is discernible, which probably has to be attributed to additional

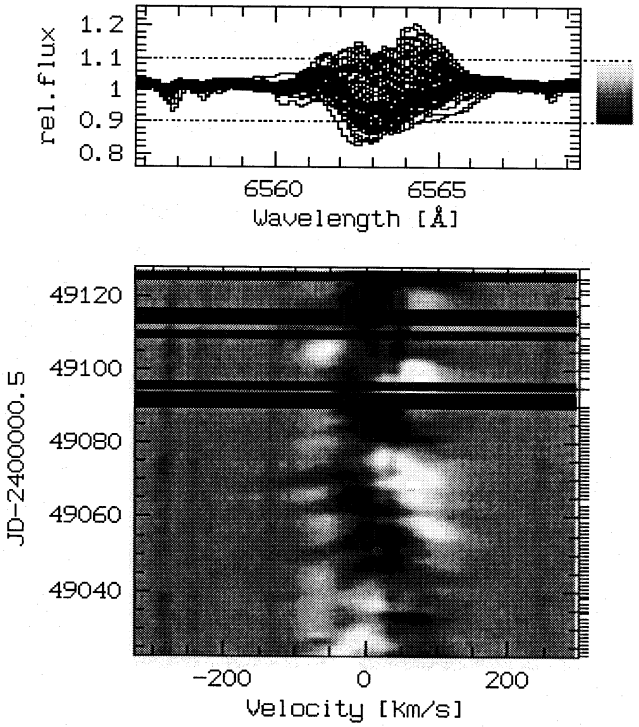

Fig. 4. Dynamical spectra of H_α of βOri in 1993 (bottom) and 1994 (top)

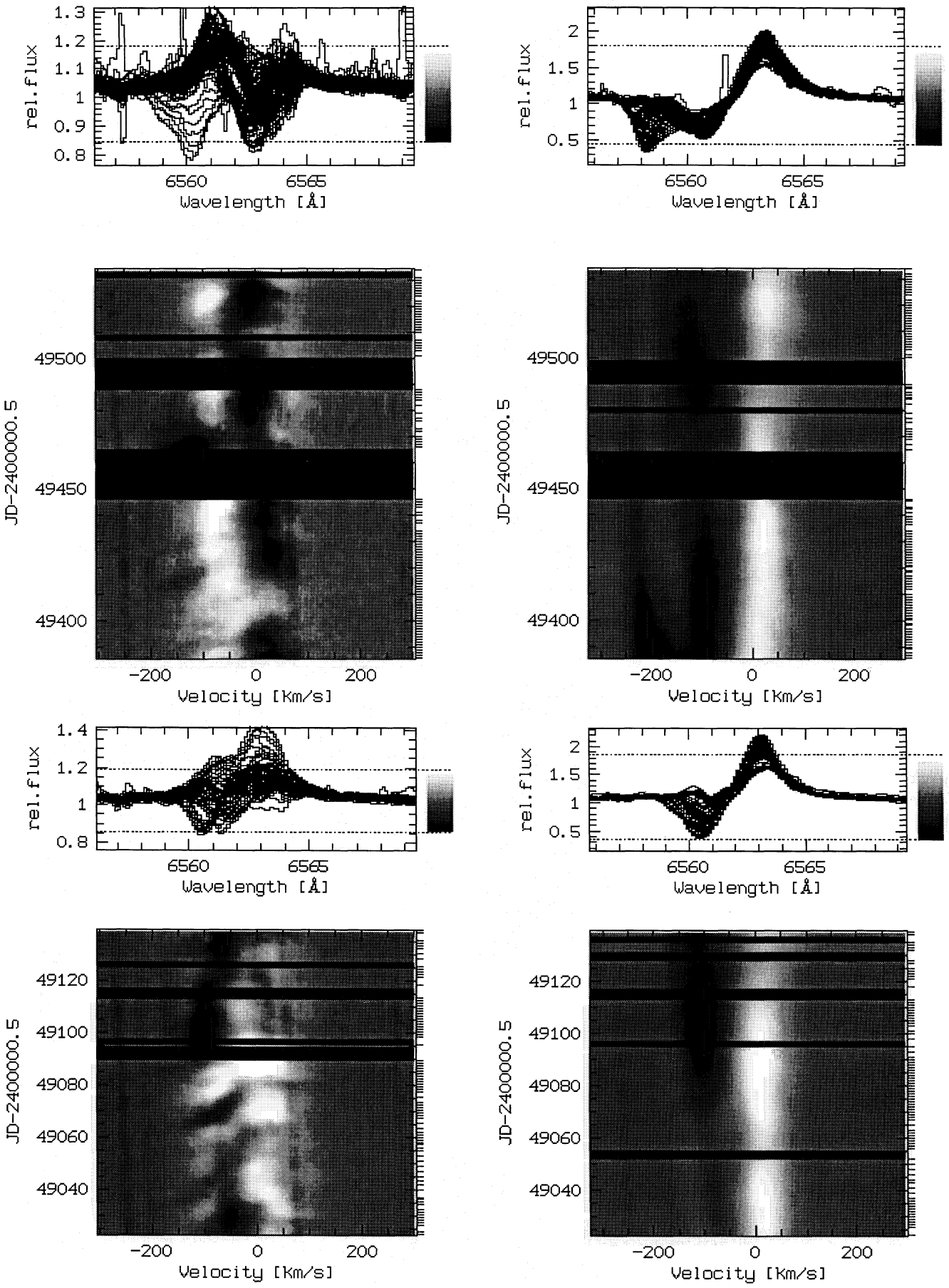

Fig. 5. Dynamical spectra of H_α of HD 96919 in 1993 (bottom) and 1994 (top)

Fig. 6. Dynamical spectra of H_α of HD 92207 in 1993 (bottom) and 1994 (top)

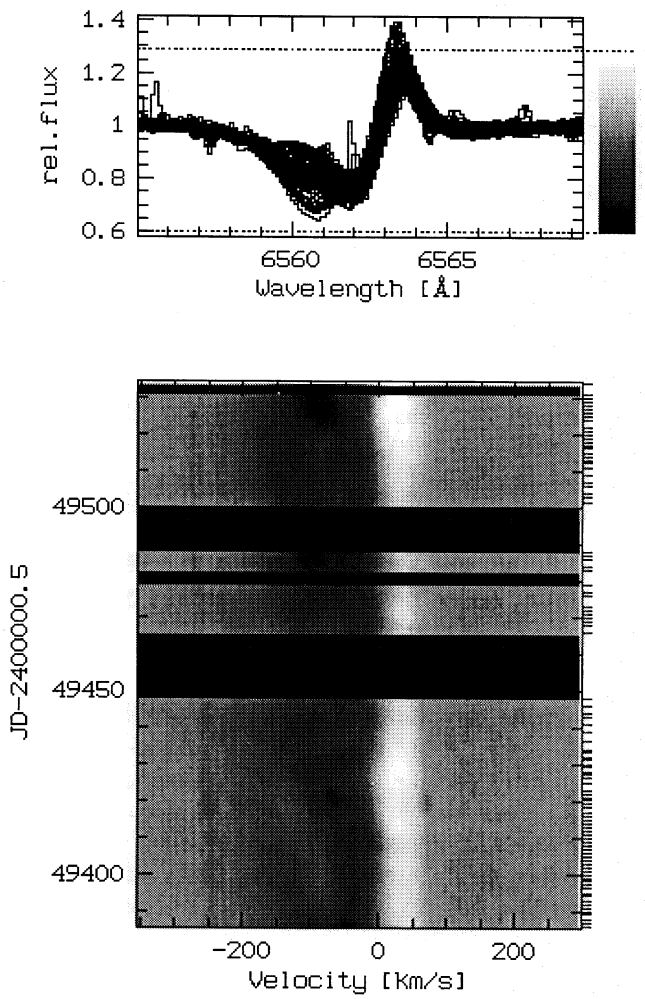

Fig. 7. Dynamical spectrum of H_α of HD 100262 in 1994

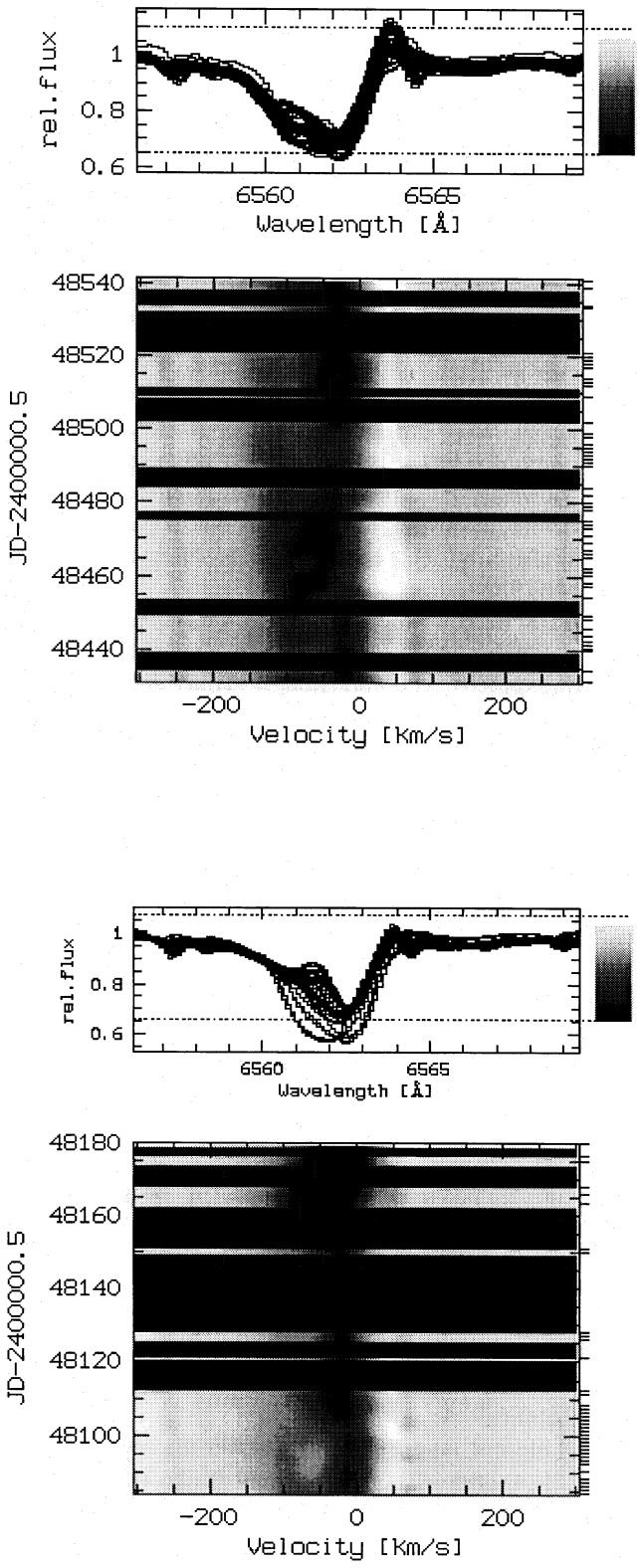

Fig. 8. Dynamical spectra of H_α of αCyg in 1990 (bottom) and 1991 (top)

emission, too. This is strongly supported by the observation of the bona fide undisturbed photospheric absorption profiles around MJD 48515 (1991). Therefore H_α variations in αCyg are also due to variable double-peaked emissions as found before for the objects without P Cyg profile in H_α.

The striking similarity of the time series of αCyg and *HD 100262* (Fig. 7) – two stars with almost identical stellar parameters – demands that the latter time series be examined with respect to double-peaked emission. Indeed, in addition to the obvious variable red-shifted emission (+20 km s^{-1}), variability located quite symmetrically about the systemic velocity in the blue at −80 km s^{-1} is seen and is mainly due to additional emission. This holds even more if the analogy to αCyg in the run of the blue side of the undisturbed photospheric profile is accepted.

HD 92207 (Fig. 6) also shows clear P Cyg profiles with variable emission and absorption. Additional extraordinary events like the propagating absorption at −230 km s^{-1} in 1994 are discussed below in Sect. 7.4. The P Cyg emission is red-shifted by some +20 km s^{-1} with respect to the systemic velocity. In 1993 a 15 % emission at −110 km s^{-1} was observed to develop into

an absorption increasing in depth over the period of observation to 60 % relative to continuum but keeping the position of maximum absorption fixed at -110 km s^{-1}. Surprisingly no propagation of this prominent absorption is measurable. The apparent effect of a propagating blue edge is due to the deepening only. The same effect was seen in 1994 in reverse order: an already present absorption at -90 km s^{-1} faded in the course of our run from 60 % to 20 % and, beginning around MJD 49480, deepened again at -110 km s^{-1} down to 35 %, both without any clear outward propagation.

A similar situtation was observed in αCyg when in 1991 between MJD 48440 and 48500 a blue edge of a weak absorption seemed to accelerate from -140 km s^{-1} to -180 km s^{-1}. This would translate into a travelled distance of 10 stellar radii if a mean velocity of -160 km s^{-1} is adopted for the propagating material. However, unless no discrete absorption component is associated with the observed accelerating blue edge, the propagation may also be attributed to a comparable effect as discussed above for HD 92207.

Therefore, we conclude that all monitored BA supergiants do show variability in H_α localized quite symmetrically about the systemic velocity. This variability is mainly due to variable additional blue and red emission superimposed on almost constant photospheric and/or wind profiles.

7.2. *Amplitudes of variability*

As can be seen from the general discussion above, a localization and quantification of variability is important for time-series analyses. To measure the line-profile variability quantitatively 'temporal variance spectra' (TVS) were computed according to Fullerton (1990):

$$(\mathrm{TVS})_i = \sigma_0^2 \frac{1}{N-1} \sum_{j=1}^{N} \left(\frac{S_{ij} - \bar{S}_i}{\sigma_{jc}\sqrt{S_{ij}}} \right)^2$$

with S_{ij} the normalized intensity of the ith pixel in the jth spectrum, $\bar{S}_i$ the weighted mean of the normalized intensity, σ_{jc} the inverse of the S/N of spectrum j measured in a continuum band, and σ_0 the inverse of the rms S/N of the time series. To compare line-profile variations of different objects $(\mathrm{TVS})^{1/2}$ is used in the following because it scales linearly with the spectral variations. In Fig. 9 the $(\mathrm{TVS})^{1/2}$ around H_α are shown in percent. Levels of significance for variability are given as horizontal lines for a 95 % probability.

For all objects, independent of whether the appearance of the mean H_α profile is P Cyg-like or more like a filled-in absorption, double-peaked TVS profiles with a red and a blue peak quite symmetric about the systemic velocity and of comparable strength are discernible. The double-peaked structure is present in successive years although intensities and velocities of the peaks do show some variations. The presence of double-peaked TVS profiles is of course just a verification of the double-peaked variability discussed above. But the TVS now allow to measure the positions and the intensities of the double peaks precisely. This was done by fitting gaussians to the peaks; results are given in Table 6 together with the systemic velocity as possible center of symmetry. In the peaks typical $(\mathrm{TVS})^{1/2}$ values between 5 to 10 % are reached; in the case of HD 92207 $(\mathrm{TVS})^{1/2}$ values up to 35 % are found. At high blue velocities singular events in the wind cause strong peaks in the TVS, as found for HD 92207 in 1994 at -209 km s^{-1} with 28 % and for βOri in 1994 with a broad peak around -100 km s^{-1} with 9 % (cf. also Sect. 7.4). Positions of the peaks are not perfectly symmetric about the systemic velocities but systematically blue-shifted. This is not intuitively expected for axisymmetric systems but may be attributed to the superimposed radial velocity field of the stellar wind. A detailed modelling of line profiles is therefore needed.

Table 6. Measured characteristics of double peaks in the TVS: velocities v_{peak} and maximum values of red and blue peaks in $(\mathrm{TVS})^{1/2}$. Peaks blended by singular events in the blue are marked with b

		max [%]		v_{Peak} [km/s]		v_{sys}
Object	year	blue	red	blue	red	[km/s]
HD 91619	1994	4.5	7.9	−101	+40	−6
	1993	7.9	7.2	+7	+55	
HD 34085	1994	b	7.0	b	+55	+18
	1993	10.8	8.2	−91	+2	
HD 96919	1994	8.2	8.7	−90	+0	−24
	1993	36.7	14.2	−110	+4	
HD 92207	1994	14.4	12.5	−88	−2	−17
HD 100262	1994	7.6	7.4	−89	+20	−17
	1990	9.8	7.9	−48	+21	
HD 197345	1991	5.6	6.0	−79	+11	−1

7.3. *Time scales of variability*

A quantification of the H_α time scales of variability is difficult because of the complex pattern observed. For a crude estimate we decided to use in a first step the equivalent width of H_α measured in the fixed interval from -400 to $+400$ km s^{-1} as a tracer for variations. The H_α equivalent width is at least a good measure for the emissivity of the star's envelope and well suited if line-profile variations can be attributed to variable emission as proposed above (cf. Sect. 7.1).

Equivalent-width curves were analyzed for periods by application of the CLEAN algorithm mentioned by Schwarzenberg-Czerny (1993). This algorithm makes use of the equivalence of the classical CLEAN algorithm and least-square fits of sine functions to the observed data (Schwarz 1978) – both performing an iterative deconvolution of the window function from the time series. The algorithm was implemented in the time-series analysis context *tsa* of MIDAS. Periodograms and power spectra are computed using Lomb-Scargle statistics (Lomb 1976, Scargle 1982), which take into account for uneven sampling of the data and have a known exponential $\chi^2(2)$ probability distribution. Therefore peaks in the periodograms below a level of significance for a 99.5 % probability were rejected from the analysis.

Before, the equivalent-width curves were normalized by subtracting their mean value and were prewhitened with the ob-

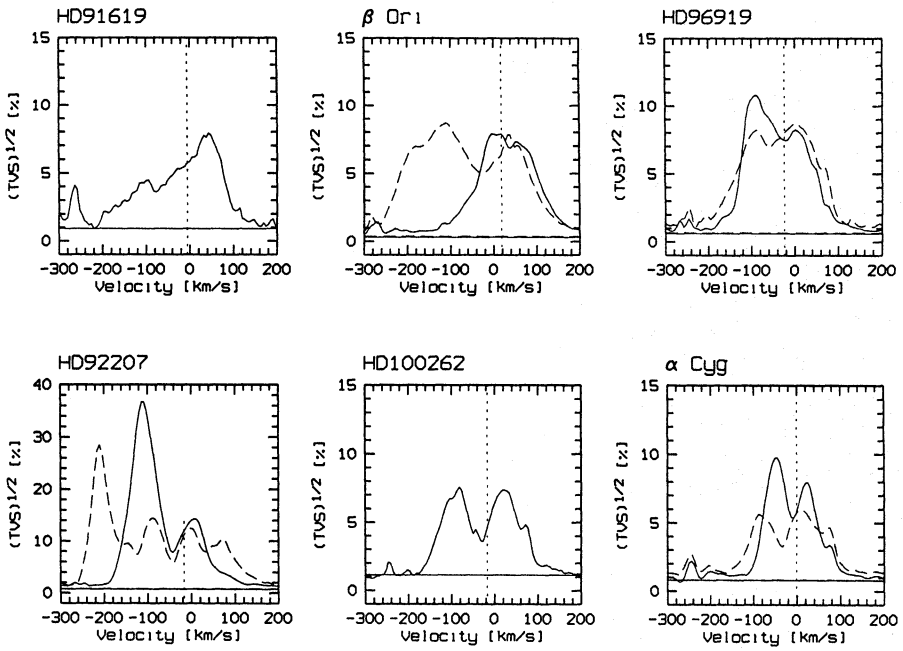

Fig. 9. TVS of H_α corresponding to Figs. 3 – 8. Solid lines = 1993 (1990 for αCyg), dashed lines = 1994 (1991 for αCyg). Levels of significance are given for a 95 % probability. Vertical dotted lines indicate the systemic velocity. Small peaks in the TVS, e.g. around -260 km s^{-1} and +80 km s^{-1}, are due to telluric lines

servation period to remove long-term trends originating mainly from singular events during the observation period. The resulting curves are shown in Fig. 10, all of which show cyclical variations with comparable peak-to-peak amplitudes ranging from 400 to 1500 mÅ.

The derived CLEANed frequencies from these equivalent-width curves are shown in Fig. 11 for all data sets from different years. The size of the symbols is scaled by the power found in the respective peaks in the periodogram. Horizontal dashed lines indicate the frequencies of expected photospheric radial fundamental pulsation modes as given in Table 4. Dot-dashed lines indicate lower limits for the rotational frequencies derived from $P_{\rm rot}/\sin i$.

For each object one strongly dominating frequency is found. This frequency seems to be reproducible from year to year as stated from the four cases where data from successive years are available.

To examine the validity of the equivalent width as a measure for variability we extended in a second step our CLEAN algorithm to the two-dimensional case in the sense that the H_α line profile at each velocity bin is treated as a time series of H_α intensity and is CLEANed in the same way as described above for the equivalent-width curves (cf. Baade 1988a, Gies & Kullavanijaya 1988). In fact, this results in CLEANed periodograms of the dynamical spectra from above, which have the advantage of preserving the information of velocity for the interpretation of the derived periods. In this case we neglected the periods found bluewards of the double-peaked structures seen in the TVS because they are expected to originate from singular events in the outer parts of the wind.

The finally derived CLEANed periods from H_α equivalent-width curves and dynamical spectra are given in days in Table 7. It is found that frequencies of the most significant peaks in the CLEAN 2D periodogram of the dynamical spectra in principal coincide with those from the 1D equivalent-width analysis. In a few cases there is a tendency to get still longer periods from the 2D periodograms, which is easily understood if the additional modulation of the integrated measure W_λ by single events is considered. Nevertheless the periods derived from the equivalent-width curves are supposed to be good measures and in the following will be referred to as the H_α time scales of the objects.

Table 7. H_α time scales in days. From the equivalent-width curves only one dominating period is found. The errors given are derived from the fit to the peaks in the power spectra. In some case of the dynamical spectra the power is equally distributed into two peaks; therefore we give two periods in these cases

		W_λ curves	dyn. spectra	
Object	year	[d]	1st [d]	2nd [d]
HD 91619	1994	12.5 ± 0.4	19	12
	1993	36.3 ± 0.9	37	
HD 34085	1994	38.5 ± 0.5	50	19
	1993	42.1 ± 0.9	45	
HD 96919	1994	35.7 ± 0.6	48	32
	1993	65.4 ± 1.3	63	
HD 92207	1994	89.3 ± 1.8	83	
HD 100262	1994	88.0 ± 5.2	91	
	1990	29.4 ± 0.4	71	40
HD 197345	1991	41.4 ± 0.8	83	43

A comparison with Table 4 shows that H_α time scales are up to a factor of 6 longer than the expected pulsation periods of radial fundamental modes. H_α time scales fall more in the regime of rotational periods as estimated from break-up velocity and $v \sin i$ (cf. Table 4).

Therefore, we conclude that rotational modulation caused by corotating surface features is an attractive source of H_α vari-

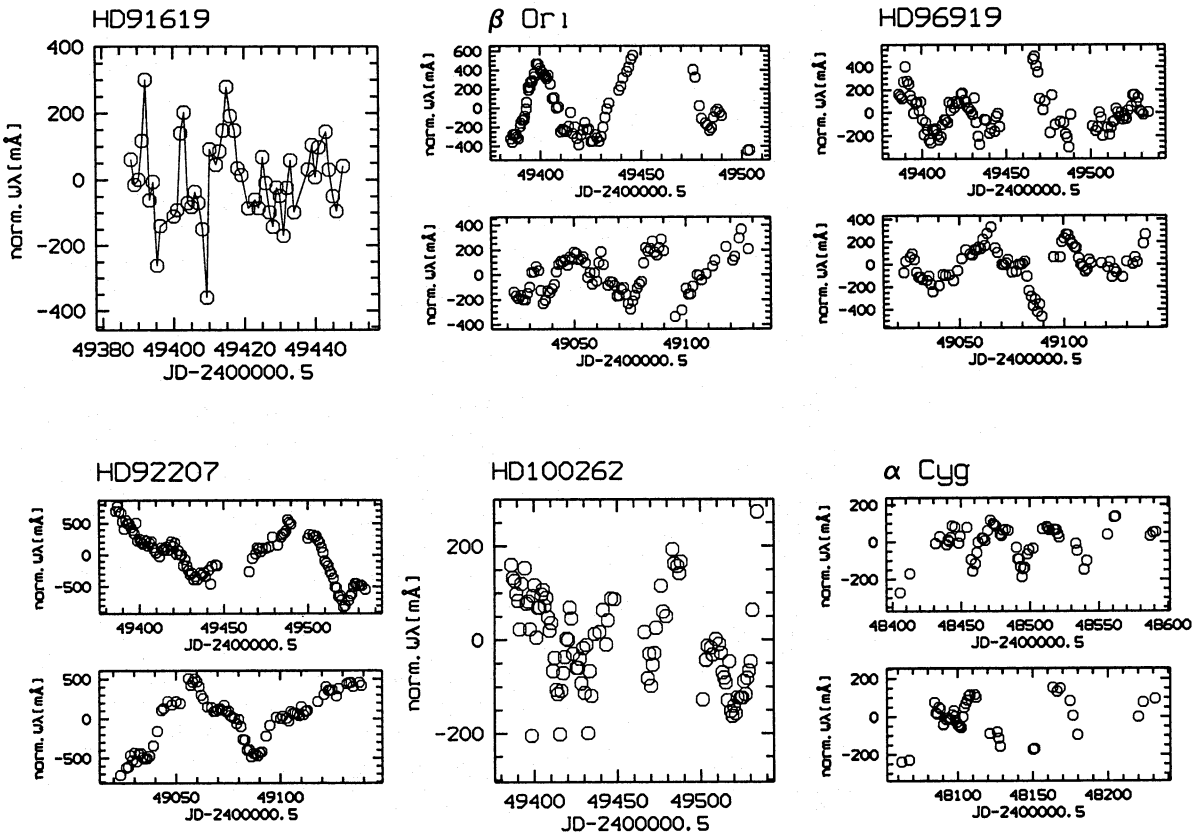

Fig. 10. Normalized and prewhitened H_α equivalent-width curves

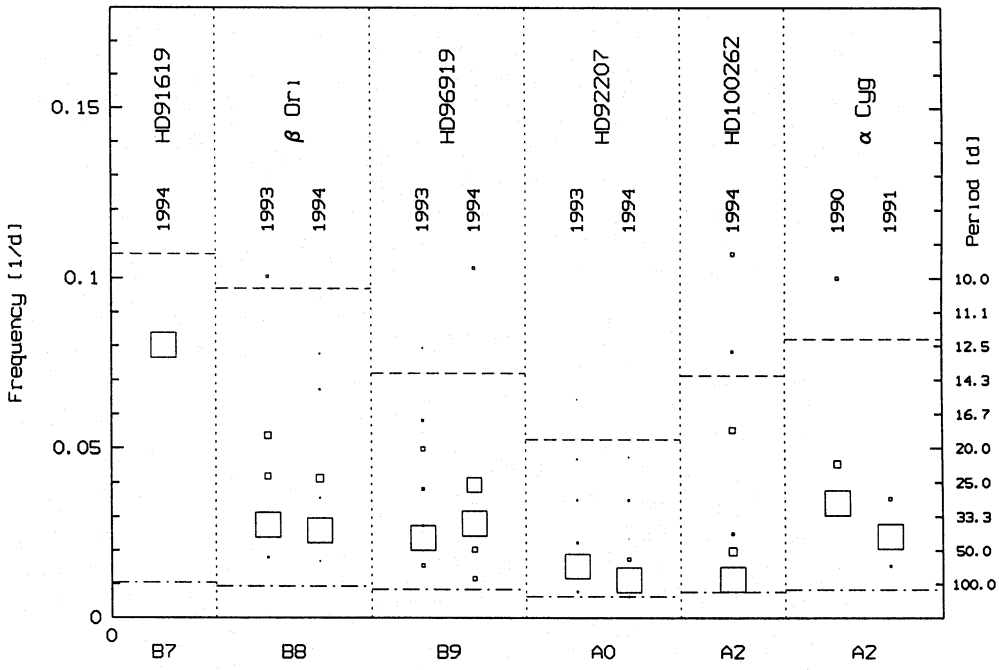

Fig. 11. CLEANed frequencies from H_α equivalent-width curves. Horizontal dashed lines indicate the frequencies of expected photospheric radial fundamental pulsation modes. Dot-dashed lines indicate lower limits for the rotational frequencies derived from $P_{\rm rot}/\sin i$

ability in BA-type supergiants. Since pulsation patterns seem to be excluded, weak magnetic structures in the sense of Underhill and Fahey (1984) are likely the prime candidate. In fact Severny (1970) reports the detection of a variable longitudinal field with a maximum value of 130 ± 20 Gauss for βOri. At the footpoint of such a field the lower boundary conditions of the wind will differ from the remaining surface, which in a natural way could give rise to a rotationally modulated lower wind region.

7.4. Extraordinary events in the wind

In addition to the dramatic overall variability in H_α, one type of special events should be pointed out: the sudden appearance of deep and highly blue-shifted absorption components. The blue-edge velocities of these events (-150 to -260 km s^{-1}) reach substantial fractions of the terminal velocities of the objects and depths (10 to 50 % relative to continuum) comparable to the observed absorptions near the systemic velocities.

A very spectacular event of this type has occurred in βOri in 1994 between MJD 49390 and 49410 with a maximum blue velocity of -260 km s^{-1} and a depth of 25 % (Fig. 4), but also in HD 91619 (1994, MJD 49410–49418, -200 km s^{-1}, 10 %; cf. Fig. 3) and HD 96919 (1993, MJD 49095–49120, -150 km s^{-1}, 20 %; 1994, end at MJD 49470, -200 km s^{-1}, 25 %; cf. Fig. 5). These absorption enhancements obviously do not propagate outwards in the wind but have the tendency to drift to lower velocities. They appear within times which are much shorter than the dynamical time scales of the wind.

The sudden appearance of absorption enhancements may be ascribed to the rotation of absorbing regions in the envelope into the line of sight or to effects in a critical ionization structure of the envelope. To examine the latter hypothesis we computed in a first step the number of accessible Lyman photons $N_{\rm lym}$ for the ionization of the wind from continua of a grid of ATLAS8 model atmospheres (Kurucz 1979) with solar composition. The stellar parameters were chosen to lie close to the limit of stability of the ATLAS8 models to simulate the proximity of the stars to the Eddington limit. This number has to be compared with the number of recombinations in the wind $N_{\rm rec}$ computed via

$$N_{\rm rec} = \int_{R_\star}^{\infty} 4\pi r^2 \beta_2(T_e) N_e^2 {\rm d}r$$

with the number of free electrons

$$N_e(r) = \frac{\dot{M}}{4\pi r^2 \mu m_{\rm H} v(r)}$$

and a standard β-type velocity law

$$v(r) = v_0 + (v_\infty - v_0)(1 - R_\star/r)^\beta$$

with an assumed start velocity $v_0 = 20$ km s^{-1}. The recombination coefficient $\beta_2(T_e)$ was taken from Spitzer (1969).

As can be seen from Fig. 12, the critical region where the number of recombinations in the wind equals the number of produced Lyman photons falls into the temperature region of the BA supergiants if a mass-loss rate of 10^{-8} $M_\odot$yr^{-1} is assumed – a value, which is reasonable for these objects as was shown by mass-loss estimates for αCyg by Lamers & Stalio (1978). However, because of the uncertainties in the Lyman continua and the detailed run of the density in the wind this estimate has to be regarded as quite qualitative and can only give a further hint on the importance of ionization in the envelopes of these stars.

Discrete absorption components or comparable features propagating outwards in the stellar wind may have been primarily expected but have only been observed once, i.e. in HD 92207 – the object showing the strongest wind characteristics in H_α. In 1994 an absorption component with a depth of 50 % relative to continuum was already present at -205 km s^{-1} in the first spectrum taken. It slowly accelerated over the whole observation run to -255 km s^{-1} while decreasing in depth to 5 %. This absorption component was also found but weaker in the obviously wind-sensitive Fe IIλ5169 line.

We traced this discrete absorption component in H_α and Fe IIλ5169 by fitting gaussians to its maximum absorption. Fig. 13 shows the measured radial velocities nicely corresponding for both lines. The asymptotic velocity $v_{\rm a}$ expected from the measured $v_{\rm inf}$ in the IUE spectra and the system velocity is $-263 - 17 = -280$ km s^{-1}. The two curves shown in the figure are visual best fits of β-type velocity laws for $\beta = 2$, $v_{\rm a} = -260$ km s^{-1} (dashed line) and $\beta = 4.5$, $v_{\rm a} = -280$ km s^{-1} (solid line), the latter giving a quite reasonable fit to the whole measured propagation curve. Unfortunately only the asymptotic part of the acceleration was observed, which leaves especially β quite uncertain. But at least from this singular event we have gained further constraints on possible moving discrete absorption components in low-velocity regimes in the sense that passing times of accelerated absorptions should be clearly shorter than the time scales of variability observed around -100 km s^{-1} for HD 92207.

8. Conclusions

For the first time an extended data set of high-quality spectra with high-resolution in wavelength and time was recorded over periods of several months in subsequent years for six late B-type and early A-type supergiants. A large wavelength range from 4 000 – 6 800 Å was covered giving great potential for analyses of the structure of the atmospheres – in this work primarily the appearance and the evolution in time of the wind-sensitive H_α line is discussed.

For all objects except for αCyg, H_α is found to show broad emission wings up to 10 % above the continuum and extended to about $\pm 1\,200$ km s^{-1}. Due to the lack of strong line emission in H_α the electron-scattered photons are expected to originate in deep atmospheric layers as described by Hubeny & Leitherer (1989).

The observed H_α variability is presented using dynamical spectra and is characterized by means of temporal variance spectra TVS and time scales derived with a CLEAN technique from equivalent-width curves and dynamical spectra.

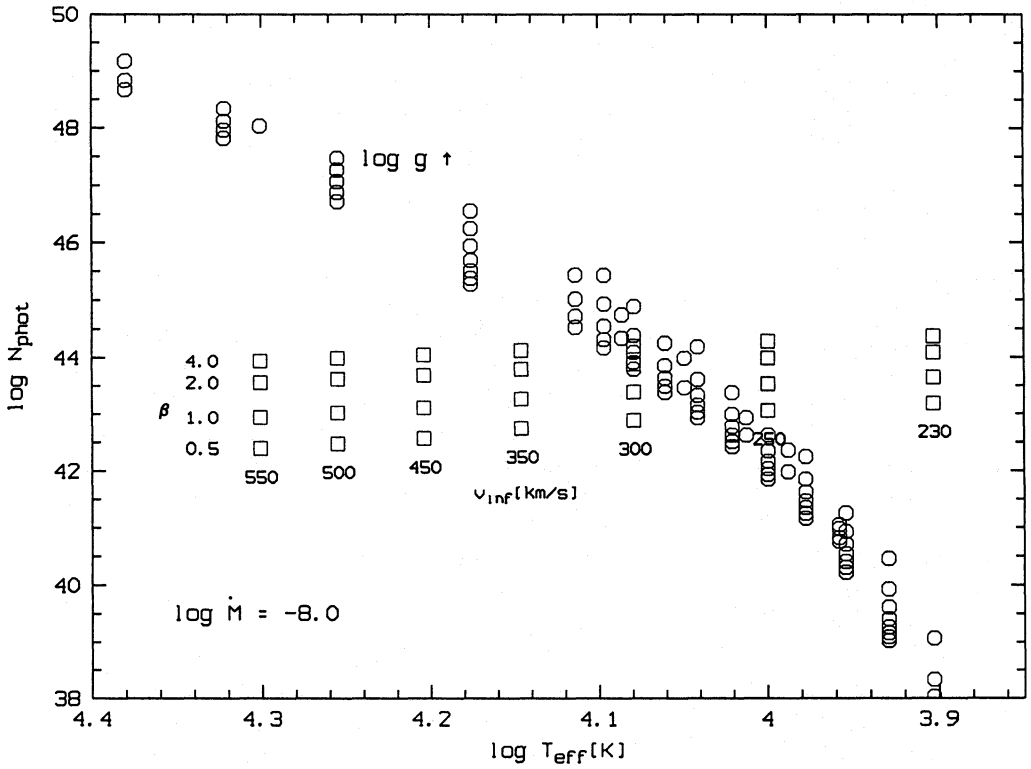

Fig. 12. Number of Lyman photons (circles) from ATLAS8 models close to instability and number of recombinations (squares) for a mass-loss rate of $\log \dot{M} = -8$ and different velocity laws versus $T_{\rm eff}$ in the region of BA supergiants

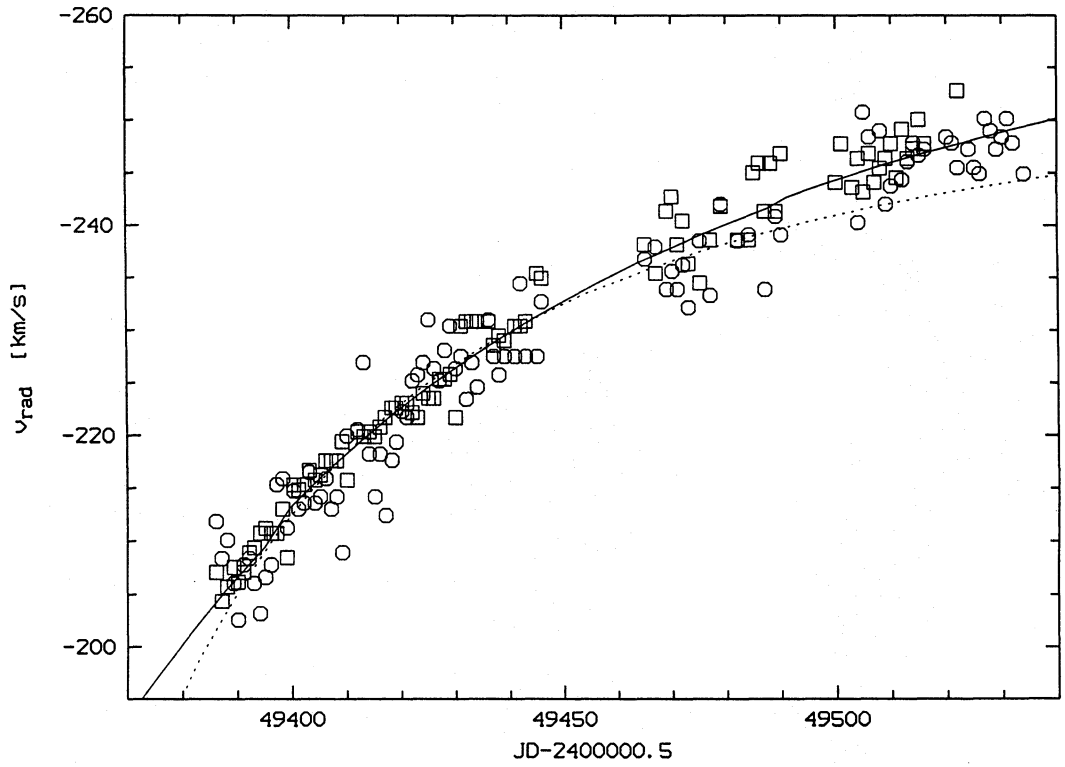

Fig. 13. Trace of the discrete absorption component observed in 1994 in HD 92207. Velocities are measured in H_α (squares) and Fe IIλ5169 (circles) by fitting of gaussians. The lines are best fits with β-type velocity laws for $\beta = 2$, $v_a = -260$ km s^{-1} (dashed line) and $\beta = 4.5$, $v_a = -280$ km s^{-1} (solid line)

From the variability in general it must be concluded that the often used steady-state, spherically symmetric approach for modelling H_α in the wind of these objects is at least not a complete one.

Variability in H_α is found to be quite symmetric about the systemic velocity and is mainly due to variable blue and redshifted emission superimposed on almost constant photospheric and/or wind profiles. These double-peaked emissions with V/R variations are interpreted in terms of axial symmetry in the extended envelopes of these objects.

Time scales of variability are up to a factor of 6 longer than expected radial fundamental pulsation periods and fall in the region of rotational periods. Therefore, rotation is thought to be a major modulation mechanism for producing V/R variations. Corotating weak magnetic surface structures are suggested as source for a rotationally modulated lower wind region.

The sudden appearance of non-propagating blue-shifted absorptions in H_α is a strong argument for the important rôle of the probably critical ionization structure of the envelopes. Outwards propagating discrete absorption components were observed only once in HD 92207 and favour a flat ($\beta = 4.5$) velocity law for a radiation-driven wind.

As a by-product from the obtained high S/N spectra three so far unidentified weak emission lines were found in the optical spectral range at 5593.27 ± 0.09 Å, 6172.66 ± 0.14 Å and 6318.21 ± 0.10 Å.

Starting from the results presented in this work, the underlying photospheric variability and its possible connection to H_α variability will be examined on the basis of the large number of lines formed in deeper regions of the atmosphere. Oscillation analyses based on photospheric lines will be presented in a forthcoming paper and will have to be compared with the H_α time scales derived above.

A detailed modelling of the presented H_α-line profiles and their variations will be of great importance for using H_α as a diagnostic tool for the physics of BA-type supergiants.

An extension of the spectroscopic long-term monitoring to earlier spectral types will be of great interest to fill the gap to the observations of Baade (1988b), who already had stated *cyclic* variations for some OB stars.

Acknowledgements. We would like to thank the staff at La Silla Observatory for the kind assistance during the observations. We are particularly grateful to Prof. Schmidt-Kaler for making available the Bochum 60-cm telescope for 22 nights in 1994 and to Dr. Alex Fullerton for passing on his experience in time-series analyses in many discussions and for carefully reading the manuscript. This work was supported by the Deutsche Forschungsgemeinschaft (Wo 296/9-1, Wo 296/16-1,Wo 296/17-1).

References

Abt H., 1957, ApJ126, 138
Azzopardi M., 1981, Structure and Distance Modulus of the SMC from Blue Supergiants. In: D'Odorico S., Baade D., Kjär K. (eds.) Proceedings of the ESO Workshop on "The Most Massive Stars", Garching, p. 227
Baade D., 1988a, Doppler Imaging of variable early-type Stars. In: Cayrel de Strobel G., Spite M. (eds.) IAU Symp. 132, Kluwer, p. 193
Baade D., 1988b, Ground-based Observations of intrinsic Variations in O, Of, and Wolf-Rayet Stars. In: Conti P., Underhill A. (eds.) Monograph Series on non-thermal Phenomena in Stellar Atmospheres: O stars and Wolf-Rayet stars, p. 137
Burki G., 1978, A&A 65, 357
Ebbets D., 1982, ApJS 48, 399
Fath E.A., 1935, Lick Obs. Bull. 17, 115
Fullerton A., 1990, PhD. Thesis, University of Toronto
Gautschy A., 1992, MNRAS 259, 82
Gies D.R., Kullavanijaya A., 1988, ApJ 326, 813
Gilheany S., 1991, Vistas Astron. 34, 249
Groth H.G., 1972, A&A 21, 337
Hensberge H., Verschueren W., 1990, A&A 240, 216
Hubeny I., Leitherer C., 1989, PASP 101, 114
Kiriakidis M., Fricke K.J., Glatzel W., 1993, MNRAS 264, 50
Kurucz R.L., Peytremann E., 1975, A Table of Semiempirical gf Values, SAO Special Report 362, Cambridge
Kurucz R.L., 1979, ApJS 40, 1
Lamers H.J.G.L.M., Stalio R., 1978, ApJ 223, 207
Lomb N.R., 1976, ApJSS 39, 447
Lovy D., Maeder A., Noëls A., Gabriel M., 1984, A&A 133, 307
Lucy L.B., 1976, ApJ 206, 499
Maeder A., Rufener F., 1972, A&A 20, 437
Mandel H., 1988, High Resolution Spectroscopy with a fiber-linked Echelle Spectrograph. In: Cayrel de Strobel G., Spite M. (eds.) IAU Symp. 132, Kluwer, p. 9
Paddock G.F., 1935, Lick Obs. Bull. 17, 99
Reid A.H.N., Bolton C.T., Crowe R.A., Fieldus M.S., Fullerton A.W., Gies D.R., Howarth I.D., McDavid D., Prinja R.K., Smith K.C., 1993, ApJ 417, 320
Rosendhal J.D., 1970a, ApJ 159, 107
Rosendhal J.D., Wegner G., 1970b, ApJ 162, 547
Rosendhal J.D., 1972, ApJ 178, 707
Rosendhal J.D., 1973a, ApJ 182, 523
Rosendhal J.D., 1973b, ApJ 186, 909
Sanford R.F., 1947, ApJ 105, 222
Scargle J.H., 1982, ApJ 263, 835
Schaller G., Schaerer D., Meynet G., Maeder A., 1992, A&ASS 96, 269
Schmidt-Kaler Th., 1982. In: Landolt-Börnstein, Neue Serie, Gruppe VI, Vol. 2b, Springer, p. 455
Schwarz U.J., 1978, A&A 65, 345
Schwarzenberg-Czerny A., 1993, Analysis of Astronomical Time Series. In: Grosbøl P.J., de Ruijsscher R.C.E. (eds.) ESO Conference and Workshop Proceedings, p. 47
Severny A., 1970, ApJ 159, L73
Spitzer L., 1969, Diffuse Matter in Space. In: Marshak R.E. (ed.) Interscience Tracts on Physics and Astronomy 28, p. 117
Stahl O., Mandel H., Wolf B., Gäng Th., Kaufer A., Kneer R., Szeifert Th., Zhao F., 1993, A&ASS 99, 167
Sterken C., 1976, A&A 57, 361
Talavera A., Gomez de Castro A.I., 1987, A&A 181, 300
Underhill A.B., Fahey R.P., 1984, ApJ 280, 712
Wolf B., Sterken C., 1976, A&A 53, 355
Wolf B., Mandel H., Stahl O., Kaufer A., Szeifert Th., Gäng Th., Gummersbach C.A., Kovács J., 1993, ESO Messenger 74, 19

This article was processed by the author using Springer-Verlag LaTeX A&A style file version 3.